# Airport Detection in SAR Images Via Salient Line Segment Detector and Edge-Oriented Region Growing

Jun Tu , Fei Gao , Jinping Sun , *Member, IEEE*, Amir Hussain, and Huiyu Zhou

*Abstract*—Airport detection in synthetic aperture radar (SAR) images has attracted much concern in the field of remote sensing. Affected by other salient objects with geometrical features similar to those of airports, traditional methods often generate false detections. In order to produce the geometrical features of airports and suppress the influence of irrelevant objects, we propose a novel method for airport detection in SAR images. First, a salient line segment detector is constructed to extract salient line segments in the SAR images. Second, we obtain the airport support regions by grouping these line segments according to the commonality of these geometrical features. Finally, we design an edge-oriented region growing (EORG) algorithm, where growing seeds are selected from the airport support regions with the help of edge information in SAR images. Using EORG, the airport region can be mapped by performing region growing with these seeds. We implement experiments on real radar images to validate the effectiveness of our method. The experimental results demonstrate that our method can acquire more accurate locations and contours of airports than several state-of-the-art airport detection algorithms.

*Index Terms*—Airport detection, line segment detector (LSD), region growing, synthetic aperture radar (SAR).

## I. INTRODUCTION

SYNTHETIC aperture radar (SAR) can achieve all-day and all-weather imaging of the earth's surface [1], [2]. Currently, target detection in SAR images has received extensive concern in the field of remote sensing [3]. Airports are valuable traffic facilities, and the detection of airports is widely applied in many practical applications, such as airport navigation, aerial reconnaissance, etc. Therefore, it has received considerable attention on how to precisely extract the airport region from SAR images.

There are four major types of methods for airport detection in remote sensing images: 1) line-based; 2) image segmentation-based; 3) saliency-based; and 4) deep learning-based. The line-based methods focus on the edges of airport runways, where salient line features are significant. They generally use Hough transform, Radon transform or line segment detector (LSD) [4] to acquire line segments. The line segments classified as runway lines are then clustered to derive the airport regions [5]–[9]. However, these methods are prone to generate irrelevant line segments because of the multiplicative speckle noise and the complex scenes in SAR images. Therefore, line-based methods generally result in more false alarms. The image segmentation-based methods mainly utilize textures [10]–[13], structural features [14], and intensity information of airports [15]. The complex feature extraction process and pixel-level analysis of these methods lead to high computational costs and poor practicability. The saliency-based methods generally design saliency cues based on the detection results of line segments [16]–[20], image frequency [21], or superpixel analysis [22]–[24] to highlight the airport regions. Since airports appear quite different from the surroundings in SAR images, the saliency-based methods are able to locate the airport regions according to above saliency cues. However, large-scene SAR images contain complex objects like rivers, which may be as salient as airports. Hence, how to distinguish the airports from other salient objects becomes a very critical and difficult problem. In recent years, with the rapid development of deep learning theories [25], [26], many methods based on convolutional neural networks (CNN) have been applied to airport detection in optical images [27]–[32]. The CNN-based methods do not require a prior information or handcrafted airport features for detection. Nevertheless, deep learning-based methods require a certain number of image samples for supervised training [33]. In some cases, it is difficult to obtain sufficient large-scene SAR image samples that cover airports for training an effective network.

In various methods of airport detection, LSD is generally applied to highlight airport geometrical features. The internal design of LSD is complicated and can be roughly divided into four parts [4]. In the first part, the image gradient and the local orientation are computed pixel by pixel, where the local orientation is defined as the orientation perpendicular to the gradient

Jun Tu, Fei Gao, and Jinping Sun are with the School of Electronic and Information Engineering, Beihang University, Beijing 100191, China (e-mail: tujun@buaa.edu.cn; feigao2000@163.com; sunjinping@buaa.edu.cn).

Amir Hussain is with Cyber and Big Data Research Laboratory, Edinburgh Napier University, EH11 4BN Edinburgh, U.K., and also with the Taibah Valley, Taibah University, Medina 30001, Saudi Arabia (e-mail: A.Hussain@napier.ac.uk).

Huiyu Zhou is with the Department of Informatics, University of Leicester, LE1 7RH Leicester, U.K. (e-mail: hz143@leicester.ac.uk).

orientation. Then, all the pixels are sorted according to their gradient magnitudes. In the second part, the sorted pixels are used as initial seeds, and a region growing algorithm is applied to forming line support regions according to the local orientations and these seeds. In the third part, line support regions are approximated with rectangles. Finally, for each rectangle, a noise model is constructed and the number of false alarms (NFA) is calculated. The rectangles with low NFA are regarded as true line segments. However, traditional LSD is designed for optical images and cannot be directly applied to SAR images.

For applying LSD in SAR images, some researchers have proposed improvement methods [20], [34]. Traditional LSD uses the difference between neighboring pixel values to compute the gradient. Nevertheless, the differential gradient is not applicable for SAR images because it will be greatly affected by inherent multiplicative noise. Liu *et al.* [20] used the logarithmic gradient to construct an improved line segment detector (ILSD), but there are still a NFA in the detection results. Besides, the assumptions about the noise model in traditional LSD are completely unsuitable for SAR images. Due to the presence of speckle noise, it is usually necessary to perform initial filtering on SAR images. It implies that strong structural dependencies exist between neighboring local orientations [34]. In order to construct an LSD suitable for SAR images, LSDSAR is proposed in [34]. It uses a pure speckle noise image to calculate the noise model of the local orientations. A first-order Markov chain is introduced to model the distribution of local orientations at neighboring pixels in LSDSAR, which performs well. However, LSDSAR aims to detect all the line segments in SAR images. For the applications in airport detection, it is only desirable to detect salient line segments related to airport runways. Consequently, it is worthy of further researching to construct an effective LSD for SAR images that highlights the geometrical features of airports.

To solve the problem of high false alarms of traditional LSD algorithms in airport detection, a salient line segment detector (SLSD) based on LSD and gradient by ratio (GR) [35] is proposed in this article. On this basis, we combine the line-based and the image segmentation-based methods to propose a coarse-to-fine detection model, which can precisely detect airports from large-scene SAR images in an unsupervised way. First of all, to highlight the geometrical features of airports, SLSD is used to extract the salient line segments in the SAR images. Next, we use line segment grouping (LSG) algorithm in [20] to group salient line segments and obtain the airport support regions. Moreover, edge detection and foreground extraction are performed on the airport support regions. All pixels from the foreground nearby the edges are sorted by gradient to produce a list of seed points. Finally, all seeds with high gradients are tested recursively and the airport region is mapped by performing region growing with these seeds, according to the features of airports like scattering intensity in SAR images. The main contributions of this article are summarized as follows.

1) A novel SLSD is proposed to extract salient line segments in SAR images. This method can suppress line segments, which are not related to the airports and thus effectively highlight the edges of airport runways. Moreover, a line segment saliency is proposed and combined in our method to help extract the edges with salient line features.

2) An effective edge-oriented region growing (EORG) algorithm is designed to extract the airport contours. This algorithm makes full use of the intensity information and edge features of the airports in SAR images, which helps produce precise detection results. Furthermore, the designed seed selection method facilitates the algorithm to achieve high performance with acceptable computational complexity.

3) The proposed method is a coarse-to-fine detection model as a whole. The airport support regions are acquired by coarse detection first, and then the airport contours are extracted by fine detection nearby those regions. Therefore, this method avoids detailed pixel-wise analysis of the entire large-scene SAR images and limits the computational complexity as a result.

The remaining parts of this article are organized as follows. Section II introduces the proposed method in detail. In Section III, our method is evaluated on real SAR images. Finally, Section IV concludes this article.

## II. METHODOLOGY

This section details the flow of our proposed method. Fig. 1 shows the flowchart. The method consists of three parts: SLSD, airport support region acquisition, and EORG. First, SLSD is constructed for the input image to extract the salient line segments and utilize the linear features of the edges of the airport. Second, the salient line segments are grouped by the LSG algorithm to obtain the airport support region. Finally, according to the edge strength map and the dark foreground image of the airport support region, the EORG algorithm is designed to obtain the seeds, which are combined with the input image to precisely extract the airport contours. Next, we will introduce the three parts of our method, respectively.

### A. Salient Line Segment Detector (SLSD)

The detection of line segments in SAR images can highlight the edges of the airport runways. However, the detection results of existing methods generally contain a large number of line segments, which are not related to airports, resulting in many false alarms. In order to suppress the influence of irrelevant linear objects and reduce false alarms of line segments, we propose a novel SLSD.

As shown in Fig. 1, SLSD is mainly composed of four parts: edge detection, coarse LSD, line segment saliency map acquisition, and fine adjustment of line segments. First of all, GR is used to obtain the edge strength map of the input image. GR is essentially a ratio of exponentially weighted averages operator with the logarithmic gradient [36]. It is effective for detecting multiscale edges in SAR images. Given a point $(a, b)$, the GR is defined as

$$G_{x,\alpha} = \log \left( \frac{\int_{x=R^+} \int_{y=R} I(a+x, b+y) \times e^{-\frac{|x|+|y|}{\alpha}}}{\int_{x=R^-} \int_{y=R} I(a+x, b+y) \times e^{-\frac{|x|+|y|}{\alpha}}} \right)$$

$$G_{y,\alpha} = \log \left( \frac{\int_{x=R} \int_{y=R^+} I(a+x, b+y) \times e^{-\frac{|x|+|y|}{\alpha}}}{\int_{x=R} \int_{y=R^-} I(a+x, b+y) \times e^{-\frac{|x|+|y|}{\alpha}}} \right)$$

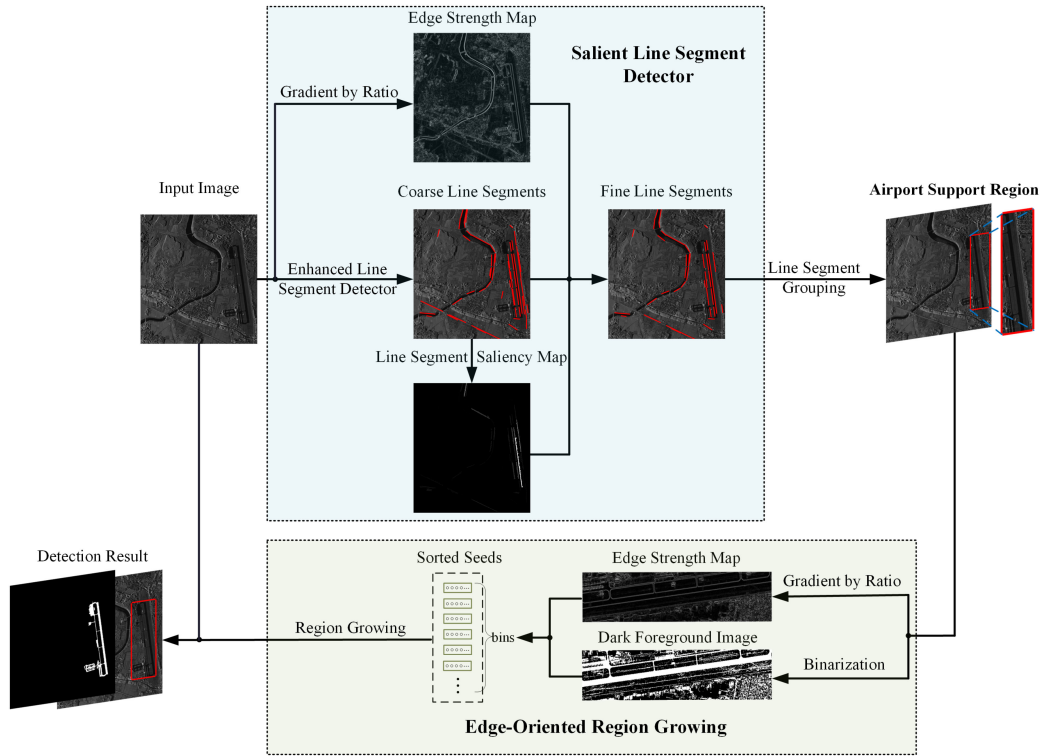$$G_{n,\alpha} = \sqrt{(G_{x,\alpha})^2 + (G_{y,\alpha})^2} \tag{1}$$

Fig. 1. Flowchart of the proposed airport detection method. It consists of three parts: SLSD, airport support region acquisition, and EORG.

where $I(a + x, b + y)$ is the gray level value of the pixel $(a + x, b + y)$ in the image $I$. $G_{n,\alpha}$ is the edge strength, which is defined as the gradient magnitude here. $G_{x,\alpha}$ and $G_{y,\alpha}$ are the horizontal and vertical gradient calculated by GR, respectively. $\alpha$ is the exponential weight parameter. It can be seen from (1) that when $\alpha$ is small, the edge strength is mainly affected by the gray level values in a small window; when $\alpha$ is large, the edge strength is mainly effected by the gray level values in a large window. Consequently, $\alpha$ is related to the scale of edges.

Second, an enhanced LSD is constructed for coarse LSD. In view of the effectiveness of LSDSAR in detecting line segments in SAR images, this part is constructed based on LSDSAR. However, LSDSAR uses GR to compute the local orientations at pixels. For the local orientation at a pixel, GR utilizes the intensity values in a large mask, which contains not only the eight-connected pixels but other pixels farther from the target pixel. It does not match the region growing with the local orientations in the eight-connected neighborhood in LSDSAR. Therefore, on the basis of LSDSAR, we improve the calculation method of local orientations for more accurate LSD. In this article, local orientations are only calculated from $2 \times 2$ masks. We define local orientations similar to [20] as follows:

$$
\begin{aligned}
G_x(a, b) &= \log \left( \frac{I(a + 1, b) + I(a + 1, b + 1)}{I(a, b) + I(a, b + 1)} \right) \\
G_y(a, b) &= \log \left( \frac{I(a, b + 1) + I(a + 1, b + 1)}{I(a, b) + I(a + 1, b)} \right) \\
O(a, b) &= \arctan \left( \frac{G_x(a, b)}{-G_y(a, b)} \right)
\end{aligned}
\tag{2}
$$

where $G_x(a, b)$ and $G_y(a, b)$ are the horizontal and vertical gradients calculated from a $2 \times 2$ mask, respectively. $O(a, b)$ is the local orientation. It should be noted that the gradient magnitudes are not calculated based on $G_x(a, b)$ and $G_y(a, b)$, but using GR of LSDSAR. In the usual LSD, the gradient magnitudes are only used for the selection of seeds in the region growing process for the acquisition of line support regions, whereas the local orientations are related to the region growing rules. Therefore, both of them do not need to rely on the same calculation method. The rest of the enhanced LSD is the same as LSDSAR, which can refer to [34]. The enhanced LSD is applied to the input image to obtain a set of line segments, which are called coarse line segments.

Third, the line segment saliency map is obtained according to the coarse line segments. For a rectangular line segment, the line segment saliency is defined as

$$
\text{LSS} = -\log(\text{NFA}) \tag{3}
$$

where NFA is the number of false alarms associated with a rectangle. Specifically, a pixel in a rectangle is aligned if it has the same local orientation as the rectangle, up to a given angle tolerance, which is generally set to $\pi/8$. Not aligned pixels are regarded as the false alarms. For a rectangle, we write $n$ for its total number of pixels and $k$ for its number of aligned pixels. We consider a rectangle with size $n$ in a pure speckle noise image and write $k_0$ for the number of aligned pixels in this rectangle. Then, the NFA is calculated by

$$
\text{NFA} = N_T \cdot \mathbb{P}(k_0 \geq k) \tag{4}
$$

where $N_T$ is the total number of possible rectangles. For an image containing $M \times N$ pixels, $N_T$ is generally derived by

$11 \cdot (MN)^{5/2}$ [4]. The probability $\mathbb{P}(k_0 \geq k)$ is computed according to the Markov chain assumption for local orientations [34]. Therefore, the smaller the NFA value, the higher the possibility that the rectangle is a meaningful line segment. To make more detailed use of the NFA values of line segments, we compute the line segment saliency based on them to highlight the edges with linear airport runways. Consequently, the definition of the line segment saliency in (3) is reasonable. The line segment saliency map consists of the linearly normalized LSS of all coarse line segments.

Finally, the coarse line segments are fine adjusted according to the edge strength map, the coarse line segments and the line segment saliency map. Specifically, the edge strength map is binarized according to the line segment saliency map to extract the edges with salient line feature. For each coarse line segment, if the center point of which is not in the edges with salient line feature, the segment is removed. Therefore, we remove the coarse line segments, which have small saliency and obtain the fine line segments. The binarization threshold is calculated by

$$w = 1 + \beta \times (1 - 2\text{LSS}_{\text{norm}})$$
$$\text{BW}_{\text{th}} = w \times \text{BW}_{\text{otsu}} \tag{5}$$

where $\text{LSS}_{\text{norm}}$ is the normalized LSS. $\omega$ is the binary weight. $\text{BW}_{\text{otsu}}$ is the binarization threshold directly obtained by the standard Otsu method [37]. $\text{BW}_{\text{th}}$ is the final binarization threshold. $\beta$ is the regulatory factor that regulates the influence of the line segment saliency on the edge extraction. When $\beta$ equals to zero, the line segment saliency has nothing to do with the edge extraction. The larger the factor $\beta$, the higher the influence of the line segment saliency on edge extraction.

### B. Airport Support Region Acquisition

To improve the accuracy of airport detection and reduce the time complexity of the algorithm, it is very necessary to obtain the airport support region to roughly locate the airport. We use the LSG method in [20] to obtain the airport support region after the line segments are acquired using the SLSD. Specifically, first, the line segments are sorted by area in the descending order. Moreover, for the line segments which are the neighbors of each other and are parallel or vertical to each other, they are clustered into the same group [20]. The bounding rectangle of each group of the line segments is the candidate airport support region. Then, we apply the nonmaximum suppression to the candidate airport support regions to reduce overlapping rectangles. Finally, according to *a priori* hypothesis that there is only one airport in a SAR image, the rectangle with the largest sum of saliency of internal line segments is determined as the airport support region.

### C. Edge-Oriented Region Growing

Since LSD generally cannot detect complete airport contours, the airport support region can only cover part of the airport. Therefore, the airport support region acquisition is essentially a rough location of the airport. Therefore, it is necessary to design an effective algorithm to conduct more precise detection for airports. Because the scattering intensity of the airport is evenly distributed, the region growing algorithm is suitable for airport detection. In addition, although the airport support region does not fully cover the airport, it can be used as a candidate region for the selection of the seeds for region growing in the airport. The full coverage of the airport region can be finally achieved based on the seeds in this limited candidate region. Therefore, we design an algorithm to select seeds from the airport support region for airport detection. The selection method of seeds directly affects the detection performance. On the one hand, if the number of seeds is too small, there will be too many fractures in the detection result. On the other hand, if the number of seeds is too large, the calculation will take too long to meet the real-time requirements in practical applications. To balance the contradiction between performance and efficiency, an EORG algorithm is proposed in this article. The procedure is shown in Algorithm 1.

The input of this algorithm is the airport support region $R$, the SAR image $I$, and a status variable $Status$. The return is the airport detection result $OutR$. The status variable $Status$ records the usage of the seeds. When a seed appears in the result of any iteration of region growing, it is updated as used. Specifically, first, GR is used to perform edge detection on the airport support region to obtain the edge strength map $gradient$. Second, on one side, the edge strength map is binarized by the Otsu method to obtain the edges of the airport support region; on the other side, the airport support region is binarized to obtain the dark foreground region $dark$. For the latter, the binarization threshold is taken as the average gray value of the largest dark connected region after Otsu binarization. Next, all the pixels in the four neighbors of the edges and in the dark foreground region at the same time are added to the set of candidate seeds $seeds$, which is written as

$$\text{seeds} = P_e \cup P_d \tag{6}$$

where $P_e$ is the pixels in the binarized edge strength map and $P_d$ is the pixels in $dark$. The seeds are sorted in descending order according to the edge strengths to obtain the seed list $OrderedListSeeds$. Note that this sort is pseudoordering, which means dividing seeds into 1024 bins in sequence, rather than strictly sorting all seeds [4]. No sorting is required inside each bin, thus the calculation time is saved. At the same time, to reduce the computational burden without significantly affecting the performance of the algorithm, the seed list $OrderedListSeeds$ only retains the first $N_{\text{bin}}$ bins. Then, the average gray difference $\tau$ of adjacent pixels is calculated as the gray tolerance of region growing. For an airport support region of size $N \times M$ pixels, $\tau$ is defined as

$$\tau = \frac{1}{N_p} \sum_{\substack{1 \leq i_1, i_2 \leq N \\ 1 \leq j_1, j_2 \leq M}} |R(i_1, j_1) - R(i_2, j_2)| \tag{7}$$

where $0 \leq |i_1 - i_2|, |j_1 - j_2| \leq 1$ and $|i_1 - i_2| + |j_1 - j_2| \neq 0$. $R(i_1, j_1)$ and $R(i_2, j_2)$ are the gray value of adjacent pixels in the airport support region. $N_p$ is the number of pairs of adjacent pixels. Subsequently, the seeds are selected in sequence from the seed list for region growing, in which the pixels with similar

**Algorithm 1:** Edge-Oriented Region Growing.

    **Input:** airport support region $R$, SAR image $I$,
           a status variable $Status$
    **Output:** airport detection result $OutR$

1   $gradient \leftarrow$ GR($R$)
2   $dark \leftarrow$ Binarization($R$)
3   $seeds \leftarrow$ SeedRegion($gradient$, $dark$)
4   $OrderedListSeeds \leftarrow$ OrderedByGradient($seeds$, $gradient$)
5   $\tau \leftarrow$ GrayTolerance($R$)
6   **foreach** $pixel\ P \in OrderedListSeeds$ **do**
7      **if** $Status(P) =$ **NOT USED then**
8          $r \leftarrow$ GrayConnected($I, P, \tau$)
9          **if** $S_r < S_R$ **then**
10             **if** ($r \in$ Neighbor($OutR$)) $\wedge$
11             ($|r_{av} - O_{av}| < \tau$) **then**
12                Add $r \rightarrow OutR$
13             **else if** $l_r > l_O \times 2$ **then**
14                $OutR \leftarrow r$
15             **else if** ($r_{av} < O_{av}$) $\wedge$ ($l_r > l_O / 2$) **then**
16                $OutR \leftarrow r$
17             **end**
18             Update($Status$)
19          **end**
20      **end**
21   **end**
22   $OutR \leftarrow$ MedianFilter($OutR$)

gray values are added to one set. The newly grown region $r$ is continuously compared with the detection result $OutR$ to obtain the final detection region. Finally, the detection region is median filtered to acquire the final airport detection result.

When we compare the newly grown region $r$ and the current detection result $OutR$, we mainly rely on the texture feature, structural feature and intensity information of the airport in the SAR image. First, on the texture feature, the airport has great intensity homogeneity. We use the gray entropy of region to measure the intensity homogeneity. The entropy of a region is calculated by

$$S = -\sum_{i=0}^{255} p_i \log_2 p_i \tag{8}$$

where $i$ is the gray level and $p_i$ is the probability of the gray level $i$ in the region. When the entropy of the newly grown region $S_r$ is less than the average entropy of the entire airport support region $S_R$, the comparison in the next step is executed. Afterward, if the absolute difference of the mean gray value of new region $r_{av}$ and the mean gray value of current detection result $O_{av}$ is lower than $\tau$, they are judged as similar gray values. If the new region is adjacent to the current detection result and the gray values are similar, the new region is added into the detection result. This step can merge the airport fragments divided by a few strong noise. Furthermore, on the structural feature, the length and aspect ratio of the airport are high. If the length of the new region $l_r$ is greater than twice the length of current

TABLE I
DETAILED INFORMATION OF DATASET

| Image | Location | Size | Spatial resolution | Polarization mode |
|---|---|---|---|---|
| #1 | Hebei Shahe | 1945×2160 | 4m | VV |
| #2 | Shanxi Pucheng | 2000×2229 | 2m | VV |
| #3 | Guangdong Shantou | 969×2344 | 4m | VV |
| #4 | Sichuan Guanghan | 1842×1024 | 1.5m | HH |
| #5 | Sichuan Mianyang | 899×1901 | 2m | HH |
| #6 | Beijing Daxing | 2238×2233 | 10m | HH |
| #7 | Beijing Nanyuan | 2233×2401 | 5m | HH |
| #8 | Beijing Nanjiao | 1181×2179 | 10m | HH |

detection result $l_O$, then the detection result is directly replaced with the new region. In addition, on the intensity information, the scattering intensity of the airport in the SAR image is quite low, which is presented as the dark brightness. Therefore, if the new region is darker and the length of new region $l_r$ is similar to the length of current detection result $l_O$, then the detection result is directly replaced with the new region. Here, two lengths are judged as similar when $l_O/2 < l_r \leqslant l_O \times 2$. In the end, after all seeds are utilized, the detection result is smoothed by the median filtering to obtain the final airport detection result.

## III. EXPERIMENTS

In this section, the dataset and the evaluation metrics used in our experiments are introduced first. Subsequently, the LSD results of different LSDs are compared. Then, the airport contour detection results and the airport location detection results of different methods are compared in detail. At last, we discuss the parameter settings and the computational efficiency of different airport detection methods. For LSD, three methods are selected for comparison with SLSD in this article. They are traditional LSD [4], ILSD [20], and LSDSAR [34], respectively. In the part of the comparative experiments for airport detection, we choose four comparison methods, namely spatial-frequency visual saliency (SFVS) [21], saliency-oriented active contour model (SOACM) [23], LSG [20], and multilayer abstraction saliency (MLAS) [24]. Among these four methods, except that LSG can only obtain the airport location detection results, the other three methods can all obtain the airport contour detection results.

### A. Dataset and Evaluation Metrics

The dataset used in this article contains eight real SAR images, whose detailed information is shown in Table I. The ground truth (GT) is manually labeled to precisely depict the airport contours according to the Google Earth images.

For the LSD results, the ratio between the number of the line segments related with the airport and the irrelevant line segments is used to evaluate the performance of the algorithms. This ratio is written as

$$\text{Ratio} = \frac{N_r}{N_{ir}} \tag{9}$$

where $N_r$ is the number of the line segments related with the airport and $N_{ir}$ is the number of the irrelevant line segments. The purpose of applying LSD in this article is to obtain the line segments related with the airport, and then combine the other steps for airport detection. Therefore, only the line segments related with the airport are considered as the correct detection result. The higher the $Ratio$, the better the algorithm can suppress irrelevant objects and highlight the geometrical features of the airport.

For the airport contour detection results, we first take precision and recall as the evaluation metrics. They are defined as follows:

$$\text{Precision} = \frac{N_{tp}}{N_d} \times 100\% \qquad (10)$$

$$\text{Recall} = \frac{N_{tp}}{N_{gt}} \times 100\% \qquad (11)$$

where $N_{tp}$ is the number of pixels in the correctly detected airport region. $N_d$ is the total amount of pixels in the airport detection result. $N_{gt}$ is the number of pixels in the real airport region. To integrate precision and recall to evaluate the algorithms, F-measure is used for experimental evaluation. It is the weighted harmonic average of precision and recall, which is defined as

$$F_\gamma = \frac{(1+\gamma^2)\text{Precision} \times \text{Recall}}{\gamma^2 \text{Precision} + \text{Recall}} \times 100\% \qquad (12)$$

where $\gamma^2$ is a weight parameter. We set $\gamma^2 = 0.3$ to weigh precision more than recall [38], [39]. In addition, these three measures do not consider the true negative counts [40]. Therefore, for more comprehensive algorithm evaluation, the mean absolute error (MAE) is added as an evaluation metric. The MAE is used to measure the average pixel difference between the detection result and GT. It can consider the proportion of the airport in the image. The smaller the MAE, the more similar the detection result is to the label. It is defined as

$$\text{MAE} = \frac{1}{|I|} \sum_x |D(I_x) - G(I_x)| \times 100\% \qquad (13)$$

where $I$ denotes the input image. $|\cdot|$ means the sum of all pixels in an image. $D$ is the detection result and $G$ is the GT. Moreover, to consider about the image-level structures and statistics of the SAR images, the structure-measure (S-measure) [41] and enhanced-alignment measure (E-measure) [42] are added as evaluation metrics. S-measure captures the structural information, which evaluates the structural similarity between the detection result and GT. E-measure jointly captures image-level statistics and local pixel matching information. The detailed calculation processes of S-measure and E-measure refer to [41] and [42].

The accuracy of the airport location is also important. We use the intersection-over-union (IoU) of between the detection result and the matched GT box to measure the performance. The IoU is defined as

$$\text{IoU} = \frac{S_\cap}{S_\cup} \times 100\% \qquad (14)$$
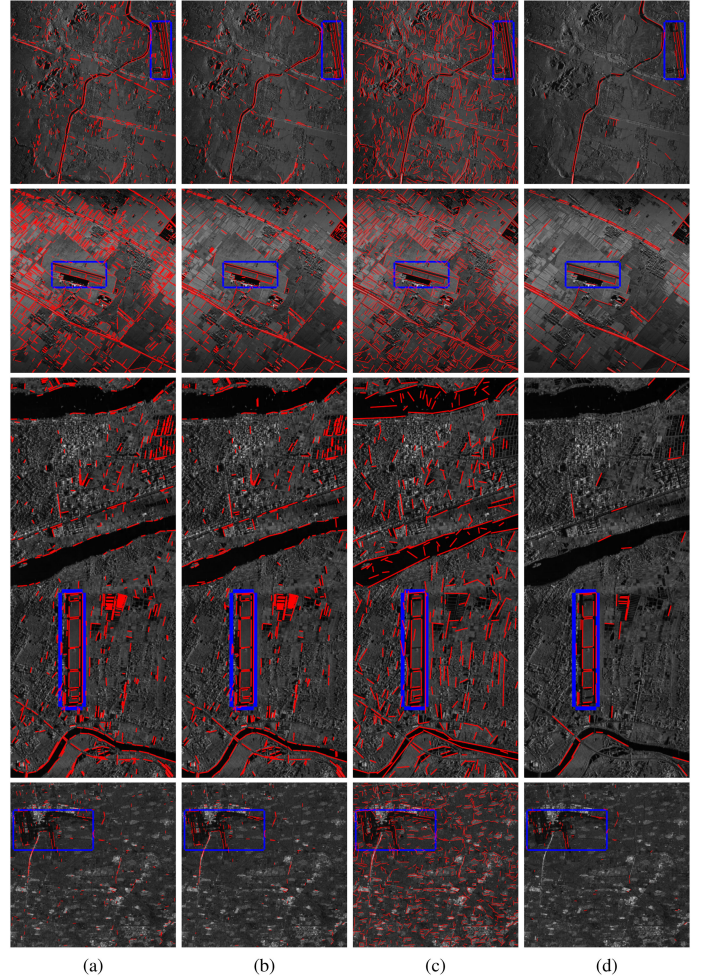


Fig. 2. LSD results obtained by (a) Traditional LSD, (b) ILSD, (c) LSDSAR, and (d) SLSD. The blue rectangles label the airport locations and the red line segments are the detection results. The line segments in blue rectangles are the line segments related to airports.

where $S_\cap$ is the amount of pixels in the intersection region between the detection result and the GT box. $S_\cup$ is the amount of pixels in the merged region between the detection result and the GT box. Obviously, the higher the IoU, the better the algorithm performance.

### B. Comparison of the LSD Results

The LSD results of four SAR images using SLSD and other LSDs are shown in Fig. 2. To highlight the airport locations, blue rectangles are artificially added here to label the correct airport locations. As shown in Fig. 2(a) and (b), ILSD has fewer false alarms on line segments than traditional LSD. ILSD adopts the logarithmic gradient on the basis of traditional LSD to highlight the edges in SAR images. Therefore, compared with traditional LSD, ILSD reduces a certain amount of false alarms on line segments. But there are still a lot of useless line segments that cannot be ignored in the detection results of ILSD. LSDSAR replaces the optical image model in the traditional LSD with the SAR image model, and introduces the first-order Markov
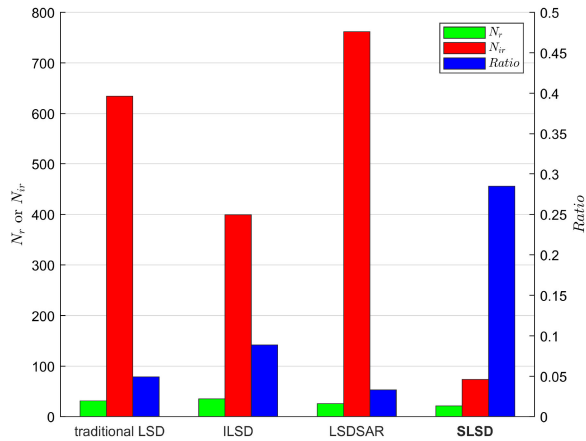
Fig. 3. Comparison of the evaluation metrics of different LSDs applied in the airport detection.

TABLE II
EVALUATION METRICS OF DIFFERENT AIRPORT CONTOUR
DETECTION METHODS

| Methods | SFVS | SOACM | MLAS | Ours |
|---|---|---|---|---|
| Precision | 31.34% | 42.53% | 50.04% | **81.11%** |
| Recall | 55.06% | 44.03% | **93.15%** | 87.74% |
| F-measure | 32.50% | 42.65% | 52.03% | **81.62%** |
| MAE | 2.13% | 1.85% | 2.14% | **0.55%** |
| S-measure | 46.73% | 49.20% | 75.79% | **88.94%** |
| E-measure | 46.58% | 57.81% | 81.41% | **96.52%** |

The bold values show the best performance among the methods with the corresponding metrics.

hypothesis about the local directions. However, LSDSAR aims to detect as many line segments as possible in SAR images. So, the detection results of LSDSAR contain a large number of line segments, which are not related to the airports, as shown in Fig. 2(c). It is shown in Fig. 2(d) that the number of line segments detected by SLSD is much less than of the other three methods. Because the line segment saliency is designed to suppress irrelevant objects in SLSD, the number of irrelevant line segments is greatly reduced. Moreover, the line segments related to airports are retained, and the geometrical features of airports are highlighted. Therefore, SLSD is able to detect the line segments related to airports in SAR images more accurately, and lay a good foundation for the subsequent extraction of the airport regions.

In order to quantitatively compare the performance of different LSDs in airport detection applications, Fig. 3 shows the average number of two types of line segments and the ratio of them in the detection results for all SAR images. Obviously, in the results of our SLSD, the number of line segments irrelevant to the airports $N_{ir}$ is greatly reduced compared to other methods. At the same time, SLSD retains a certain number of airport-related line segments $N_r$, thus obtaining the highest $Ratio$. The SLSD is designed for the detection of salient line segments, and the line segments on airport runways are generally more prominent than the line segments unrelated to the airports. Therefore, SLSD can better highlight the geometrical features of airports.

### C. Comparison of the Airport Contour Detection Results

SFVS, SOACM, and MLAS can obtain airport contour detection results. In SFVS, the images are decomposed by Gaussian pyramid first, and then the saliency maps are obtained according to the grayscale feature and frequency characteristics of the images. The largest connected region after binarization of the saliency maps are the airport detection results. In SOACM, the superpixel segmentation results of the images and the LSD results are combined to acquire the saliency maps, and the rough locations of airports are obtained according to the saliency maps. The airport contours are acquired by the active contour algorithm finally. In MLAS, the superpixel-wise segmentation results and

the airport support regions obtained by LSG are utilized to design a multilayer extraction structure to obtain the saliency maps. The largest connected region after binarization of the saliency maps are extracted as the airports.

Figs. 4 and 5 show the detection results of the proposed method and three comparison methods. It can be observed from Fig. 4(b) that the detection results of SFVS are not satisfied and appear some errors. The performance of SFVS is greatly affected by other dark and narrow regions and other prominent regions, so that roads and narrow rivers are easily mistaken for airports, as shown in the second and third images in Fig. 4(b). And the prominent lake is also mistaken for airport in the fifth image in Fig. 4(b). This is because SFVS only uses the grayscale feature and edges of airports as the main basis for airport detection. Nevertheless, the results in Fig. 5(b) are better because the images contain less other dark or prominent regions. As shown in Fig. 4(c), the detection results of SOACM are relatively precise, because it adopts an active contour model for precise iteration after locating the airports. However, because SOACM only uses simple saliency to locate the airports, once the positioning is not accurate, the final result will have no relation to the airports, as shown in the second image in Fig. 4(c) and the last two images in Fig. 5(c). As shown in Fig. 4(d) and (e) and Fig. 5(d) and (e), on our dataset, both MLAS and the proposed method can correctly detect the airports. Both methods make full use of the line segments gathered at the edges of airports. But what MLAS ultimately uses is superpixel-wise analysis, instead of pixel-wise detection in EORG in this article. Superpixel-wise analysis has large errors near the edges of airports. In comparison, the detection results of the proposed method are obviously closer to the real airport regions.

Table II shows the average value of each evaluation metric of each method on our dataset. Except for MAE, the higher the values of the other five evaluation metrics, the better the algorithm performance. It can be observed that our method achieves high performance in all kinds of metrics. Both SFVS and SOACM have serious false detection on our dataset, so that the performance in all metrics except MAE is much lower than our method. The following focuses on the detailed comparison between MLAS and our method. Observed from the first two metrics, although the recall of MLAS is higher than ours, its precision is much lower. This shows that there are more wrongly detected regions in the results of MLAS, because the superpixel
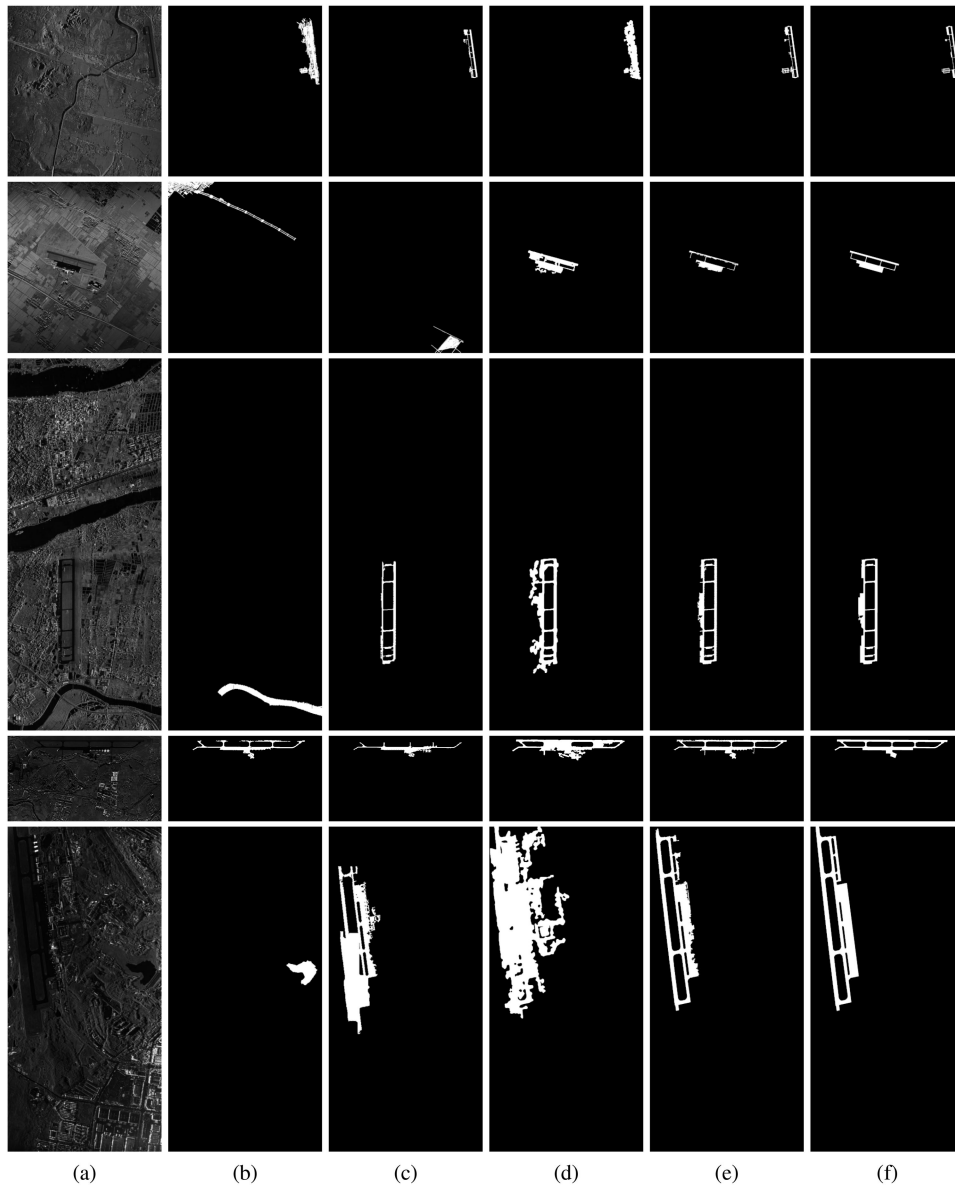
Fig. 4. Comparison of airport contour detection results obtained by different methods. (a) Original images of Image #1-#5 (top to bottom), (b) SFVS, (c) SOACM, (d) MLAS, (e) our method, and (f) GT. Note that there are some complete error results in (b) and (c).

analysis used in MLAS is easier to cover wider regions than the pixel-wise analysis in our method. F-measure integrates precision and recall. The too low precision of MLAS makes F-measure much lower than our method. The F-measure of MLAS is only 52.03%, whereas the F-measure of our method can reach 81.62%. Observed from the fourth metric MAE, the value of MAE is generally low due to the small proportion of the airport in each image. The MAE value of our method is the lowest, indicating that the difference between the detection results and GT is quite small. The S-measure of our method is as high as 88.94%, which is higher than that of all other methods. It indicates that the airport structure information retained by our method is the most complete, as shown in the comparison between the results and GT in Fig. 4(e) and (f) and Fig. 5(e) and (f). The E-measure of our method is 96.52%, which also achieves the highest level among all methods. It shows that our

detection results can match the GT very well in terms of global information and local details.

### D. Comparison of the Airport Location Detection Results

Next, we compare the airport location detection results of different methods. The comparison methods include SFVS, SOACM, LSG, and MLAS. In LSG, first, the ILSD is used to detect the line segments, which are grouped to obtain the airport support regions. Then, a kind of saliency are defined according to the length of line segments and the histogram contrast of the airport support regions. The most salient airport support region is selected as the airport location. For the other three airport contour detection methods, the bounding rectangle of the airport region is taken as the airport location. The comparison of the results is shown in Figs. 6 and 7. As shown in Fig. 6(b)
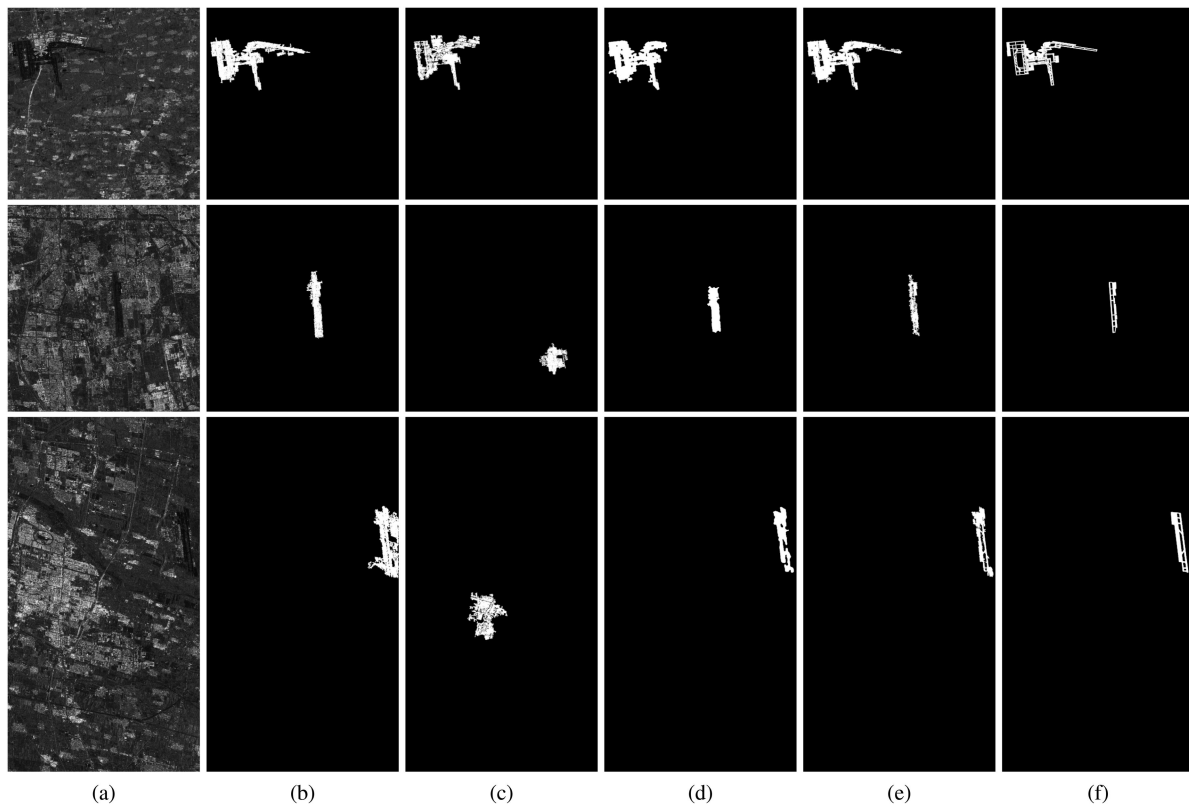
Fig. 5. Comparison of airport contour detection results obtained by different methods. (a) Original images of Image #6–#8 (top to bottom), (b) SFVS, (c) SOACM, (d) MLAS, (e) our method, and (f) GT. Note that there are some complete error results in (c).

TABLE III
IoUs OF OUR METHOD AND FOUR COMPETING METHODS

| Methods | SFVS | SOACM | LSG | MLAS | Ours |
|---------|------|-------|-----|------|------|
| IoU | 39.60% | 44.12% | 57.24% | 69.01% | **87.23%** |

The bold values show the best performance among the methods with the corresponding metrics.

and (c) and Fig. 7(b) and (c), neither SFVS nor SOACM can correctly locate the airports, so the following mainly focuses on the comparison of LSG, MLAS and the proposed method. From Figs. 6(d) and 7(d), it can be observed that in the most of the detection results, the rectangles of LSG only cover a part of the actual airport regions. This is because LSG heavily relies on the line segments, which cannot be completely consistent with the edges of airports. As shown in the first and last three images of Fig. 6(e), although the rectangles of MLAS cover the entire airport regions, they are too large and not precise enough. They cover part of the surroundings, because the superpixel-wise segmentation in MLAS cannot precisely distinguish the airports from surroundings. The detection result in the first image of Fig. 7(e) does not even cover the entire airport region. The airport runway on the far right is missing due to the inaccurate airport support regions acquired by MLAS. In contrast, as shown in Figs. 6(f) and 7(f), our method is the most precise for all images.

The average IoU of the results on all SAR images detected by each method is shown in Table III. Only the LSG, MLAS, and our method can be basically correct for airport detection on all of our dataset. The IoUs obtained by the three methods are all above 50%. Among them, the IoU obtained by our method reaches 87.23%, which is the highest. The comparison shows that MLAS is better than LSG, but the IoU is still only 69.01%. Because MLAS only introduces a superpixel-wise saliency analysis method on the basis of LSG. In the proposed method, based on the usage of LSG to obtain the airport support regions, we not only construct the SLSD, which is easier to highlight the edges of the airports, but also design a pixel-wise EORG algorithm for precise detection. Therefore, compared with LSG, our method achieves a great performance improvement, and the IoU is much higher than the other four methods.

### E. Parameter Setting

The experiments in this article involve some important parameters, so it is very necessary to explain the specific parameter settings. $\beta$ is an important parameter in SLSD, as shown in (5). The specific value of $\beta$ determines the influence of line segment saliency on the edge extraction. Furthermore, it influences the final fine adjustment of the line segments. Fig. 8 shows the average precision and recall of airport detection results of all images under different $\beta$. It can be observed that when $\beta$ is small, the two metrics basically maintain a high level. This is because $\beta$ only affects the detection result of line segments. As long as the airport support region obtained by grouping line segments covers a part of actual airport region, the subsequent EORG can precisely detect the complete airport region. When $\beta$ is greater than 0.15, the performance drops significantly. This is because
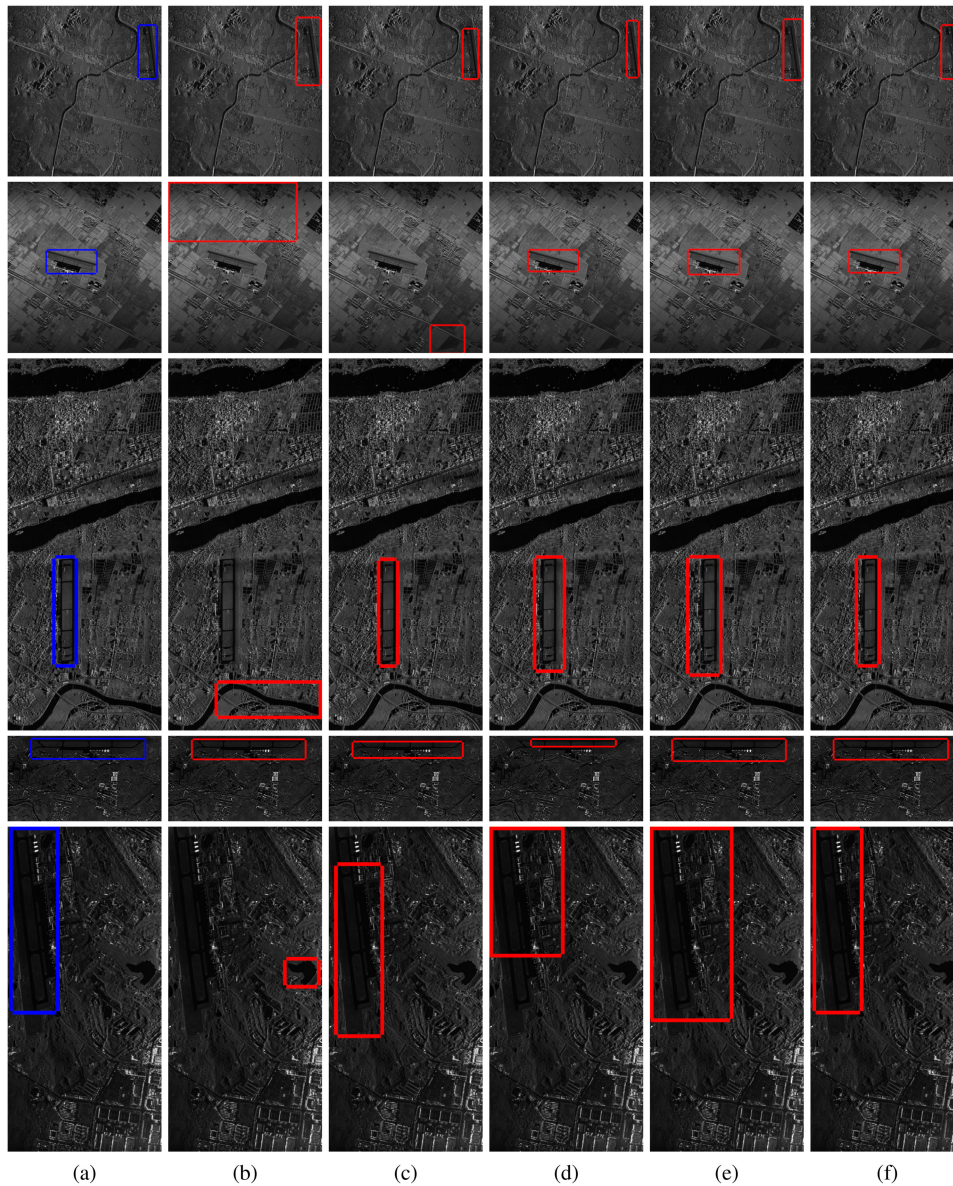
Fig. 6. Comparison of airport location detection results obtained by different methods. (a) Original images of Image #1-#5 (top to bottom), (b) SFVS, (c) SOACM, (d) LSG, (e) MLAS, and (f) our method. The blue rectangles in (a) label the correct airport locations. Only the last three methods correctly locate all airports in our dataset.

a high $\beta$ will bring about a high saliency threshold so that only a few salient line segments can be located. It makes it difficult to accurately obtain the airport support region. Therefore, $\beta$ must be maintained at a low level. In this case, our algorithm performance is robust to the fluctuation of $\beta$. In this article, the specific value of $\beta$ is 0.1.

$N_{\text{bin}}$ is an important parameter in EORG, as introduced in Section II-C. It represents the number of bins in $OrderedListSeeds$ shown in Algorithm II-C. These bins retain the seeds closest to the edges of airports. Fig. 9 shows the average precision and recall of airport detection results of all images under different $N_{\text{bin}}$. In the experiments, the range of $N_{\text{bin}}$ is set from 0 to 1024. From Fig. 9, we can find that the overall performance generally continues to improve as $N_{\text{bin}}$ gradually increases. It is because that higher $N_{\text{bin}}$ allows more

regions to be analyzed. However, for the precision metric, the performance slightly degrade when $N_{\text{bin}}$ increases from 200 to 400. It is because that large $N_{\text{bin}}$ may increase false detections. When $N_{\text{bin}}$ is greater than 500, the overall performance is stable and maintained at a high level. Therefore, to reduce the computational burden, the value of $N_{\text{bin}}$ is set to 512 in all our experiments, which is half of the original number of bins.

For GR used in this article, the exponential weight parameter $\alpha$ in (1) is taken as 2, which is consistent with [35]. It is related to the scale of the target edges. Because the airport runways are wide, the edges of airports can be reflected in both large and small scales. Therefore, $\alpha$ has very little influence on the experimental results. In addition, in the technologies related to LSDSAR used in SLSD, the parameter settings are consistent with LSDSAR. The parameters of the technologies related to
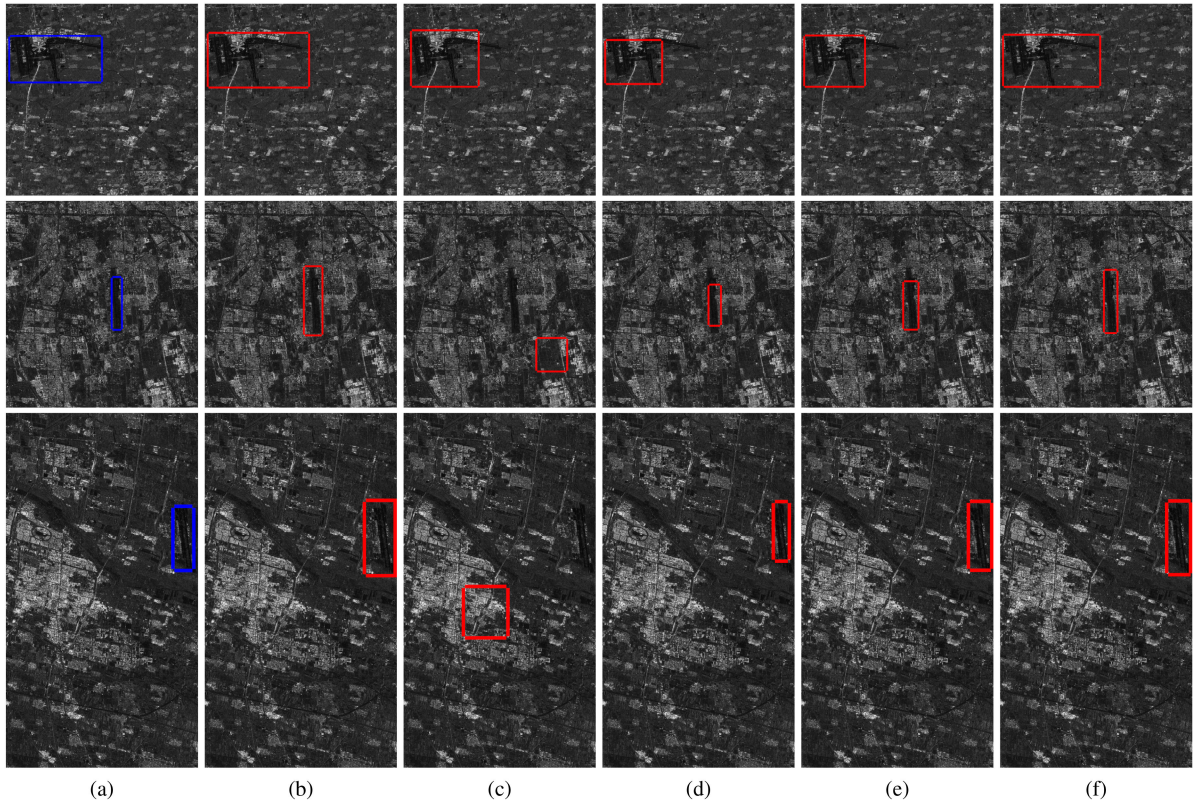
Fig. 7. Comparison of airport location detection results obtained by different methods. (a) Original images of Image #6-#8 (top to bottom), (b) SFVS, (c) SOACM, (d) LSG, (e) MLAS, and (f) our method. The blue rectangles in (a) label the correct airport locations. The results in (d) only cover a part of the actual airport regions.
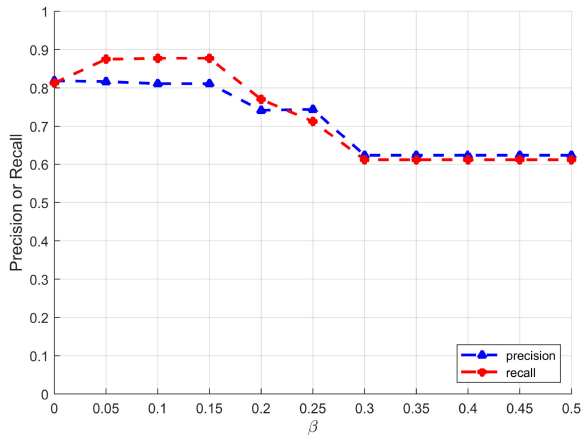


Fig. 8. Precision and recall under different values of $\beta$. The performance is great when $\beta$ is between 0.05 and 0.15.
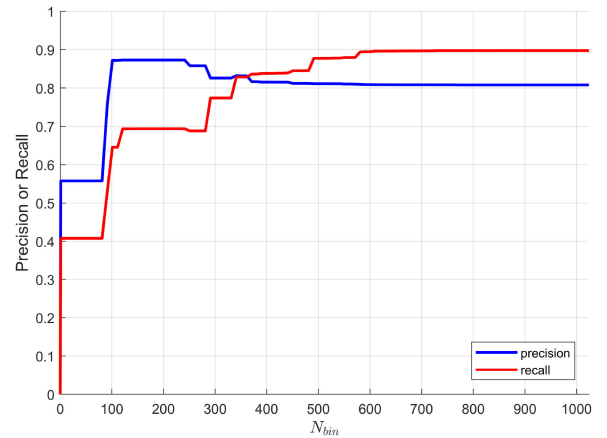


Fig. 9. Precision and recall under different values of $N_{\mathrm{bin}}$. The performance is great when $N_{\mathrm{bin}}$ is greater than 500.

LSG involved in the acquisition of the airport support regions are also consistent with them. All comparison methods use the default parameters settings described in the origin papers.

### F. Comparison of the Computational Time

The computational time of our method depends on the complexity of SLSD, airport support region acquisition and EORG. For SLSD, the enhanced LSD for coarse LSD is a linear-time algorithm as LSDSAR [35]. And other processes of SLSD such as computing the image gradient, acquiring the line segment saliency and fine adjustment of line segments only need operations proportional to the number of pixels in SAR image $N$. Therefore, the computational complexity of SLSD is $O(N)$. For airport support region acquisition, LSG method is used and the computational complexity of which is $O(N_l \log N_l)$, where $N_l$ is the number of line segments [21]. In EORG, region growing is the major part and its computational complexity

TABLE IV
COMPUTATIONAL TIME FOR DIFFERENT METHODS

| | Methods | SFVS | SOACM | LSG | MLAS | Ours |
|---|---|---|---|---|---|---|
| | Image #1 | 3.64 | 5.70 | 3.52 | 15.62 | 31.30 |
| | Image #2 | 3.39 | 7.47 | 2.60 | 16.14 | 29.02 |
| | Image #3 | 1.86 | 4.66 | 1.53 | 6.21 | 13.72 |
| | Image #4 | 1.47 | 4.27 | 1.74 | 6.57 | 6.36 |
| Time(s) | Image #5 | 1.39 | 4.13 | 1.27 | 5.22 | 14.27 |
| | Image #6 | 3.75 | 7.15 | 2.25 | 17.63 | 15.94 |
| | Image #7 | 4.04 | 8.43 | 2.48 | 21.92 | 14.15 |
| | Image #8 | 2.04 | 5.89 | 1.40 | 6.75 | 7.71 |
| | Averages | 2.70 | 5.96 | 2.10 | 12.01 | 16.56 |

is $O(N_s N \log N)$, where $N_s$ is the number of visited seeds. Because our seed selection method generates a rather small number of seeds compared to the pixels in the image. The computational complexity of EORG still can be considered as log-linear. All in all, the proposed method can run in log-linear time.

The comparison of computational time of different methods is shown in Table IV. The programs of all methods were developed in MATLAB. And all experiments were implemented on Intel Core i7-9700K CPU at 3.60 GHz and 32-GB RAM. Comparing the average time consumption for airport detection in all images with different methods using the same hardware platform, it can be observed that SFVS and LSG consume very short time. The computational time in SOACM is mainly spent on the active contour algorithm, so it takes a little long time. The superpixel-wise analysis for images in MLAS is quite time-consuming. Our method takes the longest time, which is because the region growing in EORG is very time consuming. Nevertheless, it is acceptable that the high computational loss brings a substantial improvement in detection performance.

## IV. CONCLUSION

Aiming at the airport detection in SAR images, we propose a coarse-to-fine detection model. To emphasize the geometrical features of airports and suppress the influence of irrelevant objects, a novel SLSD is proposed to detect salient line segments. Compared with other LSD algorithms, SLSD can highlight the edges of airport runways more effectively. The line segments obtained by SLSD are used to roughly locate the airport support regions. Furthermore, combined with the airport support regions, an effective EORG algorithm is designed for precise airport detection. The experimental results on real SAR images show that, by allowing a certain amount of time-consuming calculation, our method can not only locate the airports more accurately than the other comparison methods, but also extract the contours that best matches the actual airports.

## ACKNOWLEDGMENT

## REFERENCES

[1] Z. Yue et al., "A novel semi-supervised convolutional neural network method for synthetic aperture radar image recognition," *Cogn. Comput.*, 2019.

[2] F. Gao, T. Huang, J. Sun, J. Wang, A. Hussain, and E. Yang, "A new algorithm for SAR image target recognition based on an improved deep convolutional neural network," *Cogn. Comput.*, vol. 11, no. 6, pp. 809–824, 2019.

[3] F. Gao, Y. He, J. Wang, A. Hussain, and H. Zhou, "Anchor-free convolutional network with dense attention feature aggregation for ship detection in SAR images," *Remote Sens.*, vol. 12, no. 16, 2020, Art. no. 2619.

[4] R. G. Von Gioi, J. Jakubowicz, J.-M. Morel, and G. Randall, "LSD: A line segment detector," *Image Process. Line*, vol. 2, pp. 35–55, 2012.

[5] W. Wang, L. Liu, C. Hu, Y. Jiang, and G. Kuang, "Airport detection in SAR image based on perceptual organization," in *Proc. Int. Workshop Multi-Platform/Multi-Sensor Remote Sens. Mapping.*, 2011, pp. 1–5.

[6] W. Xiong, J. Zhong, and Y. Zhou, "Automatic recognition of airfield runways based on radon transform and hypothesis testing in SAR images," in *Proc. 5th Global Symp. Millimeter-Waves.*, 2012, pp. 462–465.

[7] Z. Kou, Z. Shi, and L. Liu, "Airport detection based on line segment detector," in *Proc. Int. Conf. Comput. Vis. Remote Sens.*, 2012, pp. 72–77.

[8] G. Tang, Z. Xiao, Q. Liu, and H. Liu, "A novel airport detection method via line segment classification and texture classification," *IEEE Geosci. Remote Sens. Lett.*, vol. 12, no. 12, pp. 2408–2412, Dec. 2015.

[9] Ü. Budak, U. Halıcı, A. Şengür, M. Karabatak, and Y. Xiao, "Efficient airport detection using line segment detector and fisher vector representation," *IEEE Geosci. Remote Sens. Lett.*, vol. 13, no. 8, pp. 1079–1083, Aug. 2016.

[10] C. Tao, Y. Tan, H. Cai, and J. Tian, "Airport detection from large IKONOS images using clustered SIFT keypoints and region information," *IEEE Geosci. Remote Sens. Lett.*, vol. 8, no. 1, pp. 128–132, Jan. 2011.

[11] Ö. Aytekin, U. Zöngür, and U. Halici, "Texture-based airport runway detection," *IEEE Geosci. Remote Sens. Lett.*, vol. 10, no. 3, pp. 471–475, May 2013.

[12] W. Lv, K. Dai, L. Wu, X. Yang, and W. Xu, "Runway detection in SAR images based on fusion sparse representation and semantic spatial matching," *IEEE Access*, vol. 6, pp. 27 984–27 992, 2018.

[13] Z. Zhang, C. Zou, P. Han, and X. Lu, "A runway detection method based on classification using optimized polarimetric features and HOG features for PolSAR images," *IEEE Access*, vol. 8, pp. 49 160–49 168, 2020.

[14] Z. Li, Z. Liu, and W. Shi, "Semiautomatic airport runway extraction using a line-finder-aided level set evolution," *IEEE J. Sel. Top. Appl. Earth Observ. Remote Sens.*, vol. 7, no. 12, pp. 4738–4749, Dec. 2014.

[15] S. Zhang, Y. Lin, X. Zhang, and Y. Chen, "Airport automatic detection in large space-borne SAR imagery," *J. Syst. Eng. Electron.*, vol. 21, no. 3, pp. 390–396, 2010.

[16] X. Wang, Q. Lv, B. Wang, and L. Zhang, "Airport detection in remote sensing images: A method based on saliency map," *Cogn. Neurodynamics*, vol. 7, no. 2, pp. 143–154, 2013.

[17] D. Zhu, B. Wang, and L. Zhang, "Two-way saliency for airport detection in remote sensing images," in *Proc. Int. Conf. Audio, Lang. Image Process.*, 2014, pp. 526–531.

[18] X. Yao, J. Han, L. Guo, S. Bu, and Z. Liu, "A coarse-to-fine model for airport detection from remote sensing images using target-oriented visual saliency and CRF," *Neurocomputing*, vol. 164, pp. 162–172, 2015.

[19] D. Zhu, B. Wang, and L. Zhang, "Airport target detection in remote sensing images: A new method based on two-way saliency," *IEEE Geosci. Remote Sens. Lett.*, vol. 12, no. 5, pp. 1096–1100, May 2015.

[20] N. Liu, Z. Cui, Z. Cao, Y. Pi, and S. Dang, "Airport detection in large-scale SAR images via line segment grouping and saliency analysis," *IEEE Geosci. Remote Sens. Lett.*, vol. 15, no. 3, pp. 434–438, Mar. 2018.

[21] L. Zhang and Y. Zhang, "Airport detection and aircraft recognition based on two-layer saliency model in high spatial resolution remote-sensing images," *IEEE J. Sel. Top. Appl. Earth Observ. Remote Sens.*, vol. 10, no. 4, pp. 1511–1524, Apr. 2017.

[22] D. Zhao, Y. Ma, Z. Jiang, and Z. Shi, "Multiresolution airport detection via hierarchical reinforcement learning saliency model," *IEEE J. Sel. Top. Appl. Earth Observ. Remote Sens.*, vol. 10, no. 6, pp. 2855–2866, Jun. 2017.

[23] Q. Zhang, L. Zhang, W. Shi, and Y. Liu, "Airport extraction via complementary saliency analysis and saliency-oriented active contour model," *IEEE Geosci. Remote Sens. Lett.*, vol. 15, no. 7, pp. 1085–1089, Jul. 2018.

[24] N. Liu, Z. Cao, Z. Cui, Y. Pi, and S. Dang, "Multi-layer abstraction saliency for airport detection in SAR images," *IEEE Trans. Geosci. Remote Sens.*, vol. 57, no. 12, pp. 9820–9831, Dec. 2019.

[25] W. Yan, "Detecting gas turbine combustor anomalies using semi-supervised anomaly detection with deep representation learning," *Cogn. Comput.*, vol. 12, no. 2, pp. 398–411, 2020.

[26] N. Kumar, H. K. Sardana, S. Shome, and N. Mittal, "Saliency subtraction inspired automated event detection in underwater environments," *Cogn. Comput.*, vol. 12, no. 1, pp. 115–127, 2020.

[27] Z. Xiao, Y. Gong, Y. Long, D. Li, X. Wang, and H. Liu, "Airport detection based on a multiscale fusion feature for optical remote sensing images," *IEEE Geosci. Remote Sens. Lett.*, vol. 14, no. 9, pp. 1469–1473, Sep. 2017.

[28] P. Zhang, X. Niu, Y. Dou, and F. Xia, "Airport detection on optical satellite images using deep convolutional neural networks," *IEEE Geosci. Remote Sens. Lett.*, vol. 14, no. 8, pp. 1183–1187, Aug. 2017.

[29] B. Cai, Z. Jiang, H. Zhang, D. Zhao, and Y. Yao, "Airport detection using end-to-end convolutional neural network with hard example mining," *Remote Sens.*, vol. 9, no. 11, 2017, Art. no. 1198.

[30] Y. Xu, M. Zhu, S. Li, H. Feng, S. Ma, and J. Che, "End-to-end airport detection in remote sensing images combining cascade region proposal networks and multi-threshold detection networks," *Remote Sens.*, vol. 10, no. 10, 2018, Art. no. 1516.

[31] F. Chen, R. Ren, T. Van de Voorde, W. Xu, G. Zhou, and Y. Zhou, "Fast automatic airport detection in remote sensing images using convolutional neural networks," *Remote Sens.*, vol. 10, no. 3, 2018, Art. no. 443.

[32] S. Li, Y. Xu, M. Zhu, S. Ma, and H. Tang, "Remote sensing airport detection based on end-to-end deep transferable convolutional neural networks," *IEEE Geosci. Remote Sens. Lett.*, vol. 16, no. 10, pp. 1640–1644, Oct. 2019.

[33] L. Chen *et al.*, "A new framework for automatic airports extraction from SAR images using multi-level dual attention mechanism," *Remote Sens.*, vol. 12, no. 3, 2020, Art. no. 560.

[34] C. Liu, R. Abergel, Y. Gousseau, and F. Tupin, "LSDSAR, a Markovian a contrario framework for line segment detection in SAR images," *Pattern Recognit.*, vol. 98, 2020, Art. no. 107034.

[35] F. Dellinger, J. Delon, Y. Gousseau, J. Michel, and F. Tupin, "SAR-SIFT: A SIFT-like algorithm for applications on SAR images," in *Proc. IEEE Int. Geosci. Remote Sens. Symp.*, 2012, pp. 3478–3481.

[36] R. Fjortoft, A. Lopes, P. Marthon, and E. Cubero-Castan, "An optimal multiedge detector for SAR image segmentation," *IEEE Trans. Geosci. Remote Sens.*, vol. 36, no. 3, pp. 793–802, May 1998.

[37] N. Otsu, "A threshold selection method from gray-level histograms," *IEEE Trans. Syst., Man, Cybern.*, vol. 9, no. 1, pp. 62–66, Jan. 1979.

[38] R. Achanta, S. Hemami, F. Estrada, and S. Susstrunk, "Frequency-tuned salient region detection," in *Proc. IEEE Conf. Comput. Vis. Pattern Recognit..*, 2009, pp. 1597–1604.

[39] F. Ma, F. Gao, J. Wang, A. Hussain, and H. Zhou, "A novel biologically-inspired target detection method based on saliency analysis for synthetic aperture radar (SAR) imagery," *Neurocomputing*, vol. 402, pp. 66–79, 2020.

[40] M. Cheng, J. Warrell, W. Lin, S. Zheng, V. Vineet, and N. Crook, "Efficient salient region detection with soft image abstraction," in *Proc. IEEE Int. Conf. Comput. Vis.*, 2013, pp. 1529–1536.

[41] D. Fan, M. Cheng, Y. Liu, T. Li, and A. Borji, "Structure-measure: A new way to evaluate foreground maps," in *Proc. IEEE Int. Conf. Comput. Vis.*, 2017, pp. 4548–4557.

[42] D.-P. Fan, C. Gong, Y. Cao, B. Ren, M.-M. Cheng, and A. Borji, "Enhanced-alignment measure for binary foreground map evaluation," in *Proc. 27th Int. Joint Conf. Artif. Intell.*, Jul. 2018, pp. 698–704.

**Fei Gao** received the B.S. degree in industrial electrical automation, the M.S. degree in electromagnetic measurement technology and instrument from the Xi'an Petroleum Institute, Xi'an, China, in 1996 and 1999, respectively, and the Ph.D. degree in signal and information processing from the Beihang University, Beijing, China, in 2005.

He is currently an Associate Professor with the School of Electronics and Information Engineering, Beihang University. His research interests include radar signal processing, moving target detection, and image processing.

**Jinping Sun** (Member, IEEE) received the M.Sc. and Ph.D. degrees in signal and information processing from the Beihang University, Beijing, China, in 1998 and 2001, respectively.

He is currently a Professor with the School of Electronic and Information Engineering, Beihang University. His research interests include high-resolution radar signal processing, image understanding, and robust beamforming.

**Amir Hussain** received the B.Eng. and Ph.D. degrees in electronic & electrical engineering from University of Strathclyde, Scotland, U.K., in 1992 and 1997, respectively.

Following Postdoctoral and academic positions at West of Scotland (1996–1998), Dundee (1998–2000), and Stirling Universities (2000–2018), respectively, he is currently a Professor and Founding Head of the Cognitive Big Data and Cybersecurity (CogBiD) Research Lab with Edinburgh Napier University, U.K. His research interests include cognitive computation, machine learning, and computer vision.

**Jun Tu** received the B.S. degree in electronic and information engineering from the Beihang University, Beijing, China, in 2019. He is currently working toward the M.E. degree in information and communication engineering with Beihang University.

His current research interests include object detection and synthetic aperture radar image processing.

**Huiyu Zhou** received the B.Eng. degree in radio technology from Huazhong University of Science and Technology, Wuhan, China, the M.S. degree in biomedical engineering from University of Dundee, Dundee, U.K., and the Doctor of Philosophy degree in radio technology, biomedical engineering and computer vision from Heriot-Watt University, Edinburgh, U.K.

He is currently a Professor with the School of Informatics, University of Leicester, Leicester, U.K. He has authored or coauthored widely in medical image processing, computer vision, intelligent systems, and data mining.